

Impurity-impurity interactions in Cu, Ni, Ag, and Pd

T. Hoshino

Department of General Education, College of Engineering, Shizuoka University, Hamamatsu 432, Japan

W. Schweika, R. Zeller, and P. H. Dederichs

Institute für Festkörperforschung, Forschungszentrum Jülich, D-5170 Jülich, Germany

(Received 30 July 1992)

We present systematic *ab initio* calculations for the interaction energies of impurity pairs in Cu, Ni, Ag, and Pd. The calculations are based on local-density theory and apply the Korringa-Kohn-Rostoker Green's-function method for spherical potentials. The full nonspherical charge density is used to calculate the double-counting contributions to the total energy. In particular, we calculate the nearest- and next-nearest-neighbor interaction energies of impurity pairs of the $3d$ and $4sp$ elements in Cu and Ni as well as of similar pairs of the $4d$ and $5sp$ elements in Ag and Pd: these interactions determine the ordering or segregation behavior of the alloys at finite temperatures. Comparisons are drawn with experimental phase diagrams, solid solubilities of the impurities, and also with the available information about the interaction from diffuse-scattering experiments. The physical mechanisms determining the nearest-neighbor interactions of the impurity pairs are discussed using simple model calculations based on the tight-binding method and the jellium approach: (1) The $4d$ - $4d$ interactions in Ag and Pd, being repulsive at the beginning in the $4d$ series and attractive around the middle, can be understood by considering both the changes of the d bond and the repulsive energies between different atomic rearrangement of isolated impurities and impurity pairs. For $3d$ impurity pairs with the large local moments (Cr to Co) in Cu and Ni, magnetic effects also become important. (2) The repulsive interactions of $4sp$ - $4sp$ in Cu as well as of $5sp$ - $5sp$ in Ag can be understood by the electrostatic interaction between the excess ionic charges of the impurities, being screened by the conduction electrons of the host, while the stronger repulsive interactions of $4sp$ - $4sp$ in Ni as well as of $5sp$ - $5sp$ in Pd mainly arise from the breakup of the sp - d bonds between the sp impurities and the transition-metal hosts.

I. INTRODUCTION

The interactions of point defects in solids have been the subject of numerous experimental studies in the last decade because the knowledge of the interaction is indispensable for the understanding of many basic physical processes, such as diffusion, short-range order, segregation, ordering, etc. It is obvious that the diffusion properties of impurities in metals depend strongly on the vacancy-solute interaction energies. Most interesting, from a technological point of view as well as the fundamental point of view, are the interatomic interactions in alloys, which are essential for the understanding of phase diagrams. While a huge amount of experimental data about the phase diagrams exist, the theoretical understanding of the phase stability of the alloys is one of the most important but unsolved problem in metal physics.¹ The present paper represents a small contribution to this important problem.

Recently, we have successfully calculated solution energies of impurities from first principles. The calculations are based on local-density-functional theory and apply the Korringa-Kohn-Rostoker (KKR) Green's-function method for impurities² together with a recently developed accurate total-energy formalism.³ Based on

this method, we have succeeded in calculating the vacancy-solute interaction energies in several hosts. The experimentally known interaction energies of vacancy-solute pairs in Cu, Ni, Ag, and Pd are very well reproduced by the calculations and the microscopic mechanisms have been elucidated.⁴ Further, the calculations have been applied to the interaction energies of the impurities with the probe atoms (⁹⁹Rh, ¹⁰⁰Pd, and ¹¹¹In) in Ag and Pd. By comparing our results with the available experiments, we have found in most cases good agreement with perturbed angular correlation (PAC) experiments.⁵

In this paper we use the same method to study the impurity-impurity interaction in Cu, Ni, Ag, and Pd. We have chosen the series Sc to As as the impurities in Cu and Ni and the series Zr to Sb as impurities in Ag and Pd. The reason for treating these combinations of host and impurity elements, which all belong to the same row in the periodic table, is that lattice-misfit effects, which are not included in the present calculations, should be reasonably small. The microscopic mechanisms of the impurity-impurity interactions are discussed with the help of model calculations based on the jellium model and the tight-binding approach.

In Sec. II we briefly discuss the present calculational

method. In Sec. III we discuss the calculated results for the nearest- and next-nearest-neighbor interactions of impurity pairs in Ag and Pd. In most of the cases studied here, the nearest-neighbor interaction is much stronger than the interaction at next-nearest-neighbor sites. In order to elucidate the physical mechanisms governing the chemical trends of the nearest-neighbor interactions, we have examined the following two kinds of interactions: the covalent interaction between the d orbitals on the nearest-neighbor sites⁶ and the repulsive interactions between the ion cores.⁷ In Sec. IV we describe the nearest- and next-nearest-neighbor interaction energies of the impurity pairs in Cu and Ni. The micromechanisms of the impurity-impurity interactions in Cu and Ni can also be explained analogously to Sec. III, although there are considerable differences for the strongly magnetic $3d$ impurity pairs (Cr to Co), which have their origin in the large magnetic moments of these impurities. On the basis of our calculations, we discuss in Sec. V some characteristic features of the phase diagram of the corresponding binary alloys, in particular solid solubilities of impurities and ordered structures. We also compare our results with the available effective pair interaction energies, of Ising-type models, determined from diffuse-scattering experiments. We summarize the main results of the present paper in Sec. VI.

Since the long-standing problem of predicting the phase stability of alloys from first principles has attracted large theoretical efforts, we will briefly note the differences between our more fundamental approach to calculate the interaction energies in alloys and those using the Korringa-Kohn-Rostoker coherent-potential approximation⁸ (KKR-CPA) and the Connolly-Williams approach.⁹ The present calculation, while restricted to the dilute limit, considers only configurations, the energy differences of which define uniquely the pair interactions for nearest and next-nearest neighbors.

The generalized perturbation method¹⁰ (GPM) combined with the KKR-CPA method starts from completely disordered alloys, as described quite realistically by the KKR-CPA, and then calculates the interactions by inserting two specific atoms into the CPA medium. In this way the concentration dependence of the interaction is fully included as a result of the embedding into the CPA medium. However, additional approximations cannot be avoided. While the KKR-CPA relies already on the single-site approximation being not unproblematic for alloys with charge transfer,¹¹ in the GPM the two- and more-center interactions are calculated in the frozen-potential approximation and moreover by taking only single-particle energies into account. In the present treatment, all these approximations are avoided, which has to be paid for by being restricted to the dilute limit.

In principle, the Connolly-Williams approach⁹ determines in the same spirit the interactions from different configurations. Here the results of supercell calculations with many different configurations in the unit cell are fitted by models containing two- and three-center interactions. The best fit obtained by the smallest number of parameters determines the optional model for the interactions, which can therefore not be determined uniquely.

The statistical part of the calculations, i.e., the calculation of the phase diagram from given interactions, could be performed either by the cluster variational method¹² or by the Monte Carlo method.¹³ The latter more accurate method has been used for some of the results cited in Sec. V, e.g., calculating the solubility of Co in Cu.

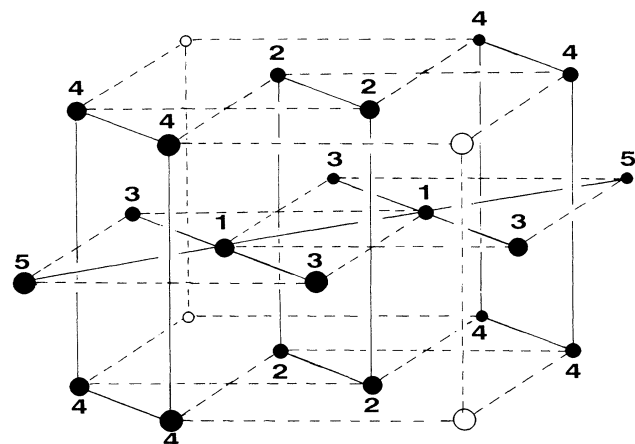
II. METHOD OF CALCULATION

In this section we summarize only briefly the main characteristic features of the calculational procedure, as it has been discussed by Klemradt *et al.*⁴ We will outline the theory for paramagnetic systems; the generalization to magnetic systems is obvious. The calculations are based on the KKR Green's-function method for the impurity calculations² and on a recently developed accurate total-energy formalism.³ In the KKR Green's-function method, the Green's function of the system is expanded in each cell into radial eigenfunctions of the local potential, assumed to be spherically symmetric within the Wigner-Seitz spheres. For the spherical potentials, we use the $l=0$ component of the full cell potential, which is constructed from the full cell charge density. All the multiple-scattering information is contained in the structural Green's-function matrix $G_{LL'}^{nn'}(E)$, which is related to the $\hat{G}_{LL'}^{nn'}(E)$ of the ideal crystal by a Dyson equation

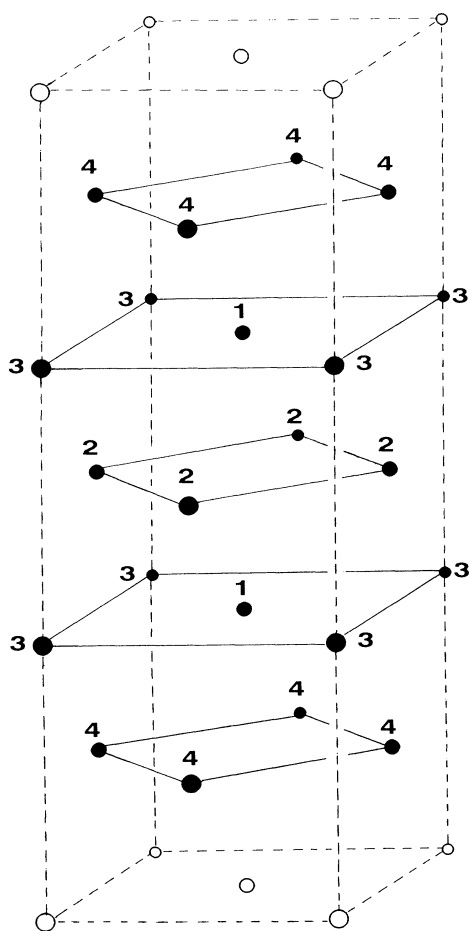
$$G_{LL'}^{nn'}(E) = \hat{G}_{LL'}^{nn'}(E) + \sum_{n'', L''} \hat{G}_{LL''}^{nn''}(E) \Delta t_{L''}^{n''}(E) G_{L''L'}^{n''n'}(E), \quad (2.1)$$

where $\Delta t_{L''}^{n''}(E) = t_{L''}^{n''}(E) - \hat{t}_{L''}^{n''}(E)$ is the deviation from the host t matrix $\hat{t}_{L''}^{n''}(E)$. The rank of G is determined by the number of perturbed potentials and the number of angular momenta taken into account.

For the present impurity systems, we calculate self-consistently all perturbed atomic potentials in the two kinds of impurity clusters shown in Fig. 1; Fig. 1(a) shows the 20-atom impurity cluster for the nearest-neighbor interaction energy and Fig. 1(b) the 22-atom impurity cluster for the next-nearest-neighbor interaction energy. In the 20- (22-) atom impurity cluster, the two impurity atoms are situated at the nearest-neighbor (next-nearest-neighbor) sites 1, whereas 18 (20) host atoms occupy the sites 2–5 (2–4) and are nearest neighbors to at least one of the impurity atoms. The maximum angular momentum l_{\max} for the Green's function is chosen to be 3. It was shown in Ref. 3 that both approximations are sufficient to obtain reliable total energies. The change of the integrated density of states, necessary to calculate the change of the single-particle energies induced by the impurities, is determined by Lloyd's formula,³ which analytically sums all perturbations of the wave functions over the whole infinite space. The energy integration is performed by a contour integral in the complex energy plane.¹⁴ The double-counting contributions for both the Coulomb and exchange energies are calculated by use of the full anisotropic charge density in each Wigner-Seitz cell.^{4,15} The integrations over the exact faceted Wigner-



(a)



(b)

FIG. 1. Two impurity clusters used in the present calculations. All the atoms are on fcc sites. (a) The 20-atom cluster of D_{2h} symmetry for the nearest-neighbor interaction. Five kind of sites are shown: one impurity site 1 in the center and four nearest-neighbor sites (2-5) adjacent to the impurity sites. (b) The 22-atom cluster of D_{4h} symmetry for the next-nearest-neighbor interaction. Four kind of sites are shown: one impurity site 1 and three nearest-neighbor sites (2-4) adjacent to the impurity sites.

Seitz cell can be performed by introducing a Heaviside function, which is equal to 1 inside and 0 outside the cell, expanded by spherical harmonics within the circumscribing sphere of the Wigner-Seitz cell. We apply density-functional theory in the local-density approximation of von Barth and Hedin with the parameters as given by Moruzzi, Janak, and Williams.¹⁶

The interaction energy E_{int} between the two B impurities in the host A is defined as the total-energy difference between two states: (1) the final state where the two B impurity atoms are located at nearest-neighbor (or next-nearest-neighbor) sites 1 and (2) the initial state where both the impurity atoms are infinitely far away. Thus E_{int} is given by

$$E_{\text{int}} = \Delta E_{BB} - 2\Delta E_{AB}, \quad (2.2)$$

$$\Delta E_{BB} = E_{BB} - E_{AA}, \quad (2.3)$$

$$\Delta E_{AB} = E_{AB} - E_{AA}, \quad (2.4)$$

where E_{XY} represents the total energy of the system with the X - Y pair in the center of the cluster and ΔE_{XY} is the excess energy with respect to the energy of the ideal A crystal. All energies E_{XY} 's are calculated using the 20- or 22-atom geometries shown in Fig. 1.

III. CALCULATED RESULTS OF THE IMPURITY PAIRS IN Ag AND Pd

In this section we discuss the calculated results for the nearest- and next-nearest-neighbor interaction energies of the $4d$ and $5sp$ impurity pairs in Ag and Pd. All the pairs considered here are nonmagnetic.

A. Impurity-impurity interactions in a noble metal Ag

Figure 2 and Table I show the calculated interaction energies between pairs of equal impurities in Ag. Table I also lists the results for Pd, discussed in the next subsec-

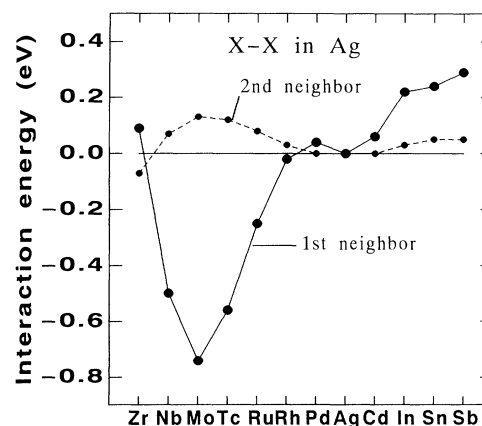


FIG. 2. Interaction energies between two identical $4d$ or $5sp$ impurities in Ag. The large solid circles (\bullet) indicate the interaction energies for the nearest-neighbor sites, and the small solid circles (\bullet) refer to the next-nearest-neighbor sites.

TABLE I. Calculated n th-neighbor interaction energies E_n^{int} ($n=1,2$) of $4d$ and $5sp$ impurity pairs (Zr to Sb) in Ag and Pd (in eV). Negative values mean attractive interaction, positive ones repulsive interaction.

Impurity	Zr	Nb	Mo	Tc	Ru	Rh	Pd	Ag	Cd	In	Sn	Sb
Host Ag												
E_1^{int}	0.09	-0.50	-0.74	-0.56	-0.25	-0.02	0.04		0.06	0.22	0.24	0.29
E_2^{int}	-0.07	0.07	0.13	0.12	0.08	0.03	0.00		0.00	0.03	0.05	0.05
Host Pd												
E_1^{int}	1.48	1.06	0.38	-0.04	-0.14	-0.05		0.00	0.18	0.67	0.87	0.90
E_2^{int}	0.06	0.08	0.11	0.09	0.05	0.01		0.00	0.00	0.04	0.05	0.07

tion. Positive energies mean repulsive interaction between the impurity atoms, negative ones attractive interaction. From Fig. 2 it is obvious that the nearest-neighbor interactions are of major importance. Following the characteristics of the chemical trends found in the calculation, the nearest-neighbor interaction energies can be classified into the following two groups.

(1) For the $4d$ - $4d$ pairs, except the impurity pairs at both ends (Zr,Pd) of the $4d$ transition-metal series, the interaction is attractive and its magnitude changes parabolically from Zr to Pd, with the minimum at Mo.

(2) For the $5sp$ - $5sp$ pairs, the interaction is repulsive and its magnitude increases with the valence difference between the impurity and host atoms. A parabolic dependence is found from Ag to In and a smaller increase from In to Sb.

It is found from the comparison between the calculated results and the observed structures of phase diagrams^{1,17-19} shown in Table II that the fundamental characteristic features of ordering systems such as AgZr, AgCd, AgIn, AgSn, and AgSb are the repulsive interactions between the nearest-neighbor impurity atoms in the host metals; this is easily expected because the atom of the impurity element becomes surrounded with the atoms of the host element as a result of the repulsive interaction of the impurity pair. Contrary to this, if the interaction between two impurities is attractive, the impurity atoms attract each other and then the binary alloys of host and impurity elements should become of segregation type; in line with this reasoning, the impurity-impurity interactions of the binary alloys AgNb, AgMo, AgRu, and AgRu, being of segregation type, are indeed attractive. Thus we may expect that the difference between solid

solution type and segregation type of the binary alloys is only distinguished by the nearest-neighbor interaction of the impurities, which can be obtained from the calculations of a dilute limit. However, the differences between the uniform solid solution and the ordered compounds, as well as those among a variety of ordered structures, depend on the more subtle interatomic interactions at the more distant neighbor sites (see Sec. V for details).

Here we will discuss the physical origins of the nearest-neighbor impurity-impurity interactions. First, we explain the interaction of $4d$ - $4d$ pairs. The basic feature shown in Fig. 2 is the strong binding of two $4d$ impurities, due to the covalent hybridization between the $4d$ states. In order to examine the chemical trends of the covalent interaction, we use the Alexander-Anderson model.^{6,20} All the information of the electronic structures of d states for two impurity atoms in a free-electron-like host can be obtained by solving a Dyson equation

$$G_{mm}^{nn'}(E) = \hat{G}_{mm}^{nn'}(E) + \sum_{n''} \hat{G}_{mm}^{nn''}(E) V_{mm}^{n''n'}(E) G_{mm}^{n''n'}(E), \quad (3.1)$$

where $\hat{G}_{mm}^{nn}(E)$ is the Green's function of the virtual bound states of the isolated impurity specified by n as

$$\hat{G}_{mm}^{nn}(E) = \frac{1}{E - E_d + i\Gamma}. \quad (3.2)$$

Γ and E_d represent the half width and energy level of the virtual bound state, respectively, of the impurity in Ag; Γ may be estimated by Heine's relation,²¹ and then E_d can be obtained by assuming \hat{N}_d of a free atom, while the covalent (interatomic) interaction V_{ddm}^{12} between two d or-

TABLE II. Experimental information about ordering, decomposition and solid solubility in binary alloys of host elements (Ag, Pd) and (Cu, Ni) and impurity elements (Zr to Sb) and (Sc to As). All data are shown in Refs. 1 and 17-19. The symbols in the table are defined as follows: +, ordered compound exists (+ +; stable up to the melting point), and E_1 should be >0 (or $\gg 0$); -, miscibility gap is found, and E_1 should be <0 ; and l, s, c , large, small, continuous solid solubility, and therefore, if c , $|E_i|$ is small, if $+ + l$, $E_1 \gg 0$ and $E_2 \geq 0$, and if $+ + s$, $E_1 \gg 0$ and $E_2 < 0$; ?, no experimental data available (the prediction is given in parenthesis); and \circ indicates the very few minor differences between observations and calculations (see text).

	Zr	Nb	Mo	Tc	Ru	Rh	Pd	Ag	Cd	In	Sn	Sb	
Ag	$\oplus + s$	$-s$	$-s$	$?(-s)$	$-s$	$-s$	c		$+l$	$+ + l$	$+ + l$	$+ + l$	
Pd	$+ + ?(l)$	$+ + l$	$+l$	l	$-s$	c		c	$+ + l$	$+ + l$	$+ + l$	$+ + l$	
	Sc	Ti	V	Cr	Mn	Fe	Co	Ni	Cu	Zn	Ga	Ge	As
Cu	$+ + s$	$+ + s$	$-s$	$-s$	$\oplus c$	$-s$	$-s$	c		$+l$	$+ + l$	$+ + l$	$+ + l$
Ni	$+ + \circ$	$+ + \textcircled{l}$	$+ \textcircled{l}$	$+c$	$+l$	$+c$	c		c	$+l$	$+ + l$	$+ + l$	$+ + \circ$

bitals on the neighboring atoms may be estimated following Harrison and Froyen.^{22,23} The d functions of two impurity atoms in jellium can be classified by the molecular orbitals $dd\sigma$, $dd\pi$, and $dd\delta$ according to their azimuthal angular momentum $l_z=0, 1, \text{ or } 2$ around the molecular axis. The $dd\sigma$ orbital is singly degenerate, and the $dd\pi$ and $dd\delta$ ones are doubly degenerate. Because of the covalent (interatomic) interaction V_{ddm}^{12} , each of these states splits into a bonding and antibonding state. Thus one would expect six different peaks. The average potential on each site can be determined self-consistently by use of Eq. (3.1) and the equations

$$V_{mm}^{nn} = U(N_d^n - \dot{N}_d^n), \quad (3.3)$$

$$N_d^n = -\frac{1}{\pi} \int_{-\infty}^{E_f} dE \operatorname{Im} G_{mm}^{nn}(E), \quad (3.4)$$

where U ($=5$ eV) is the intra-atomic Coulomb integral and \dot{N}_d^n is the d -electron number of the isolated impurity n . A more detailed discussion of Γ , V_{ddm}^{12} , and U will be given elsewhere.²⁴ Using the resultant phase shift ϕ , we can calculate the d -bond energy U_{bond}^{XX} between the two X impurity atoms,

$$(E_{\text{int}}^{\text{bond}} =)U_{\text{bond}}^{XX} = -\frac{1}{\pi} \int_{-\infty}^{E_f} dE (E - E_f) \frac{d\phi}{dE} - U[(N_d^X)^2 - (\dot{N}_d^X)^2]. \quad (3.5)$$

In order to estimate $E_{\text{int}}^{\text{bond}}$, we must also take into account the bond energies between host and impurity and host and host [as in Eq. (3.7)]. However, those bond en-

ergies may be neglected because the d orbitals of Ag are very localized like core electrons and the sp bonds are weak. The calculated covalent interaction energy (d -bond energy) is shown in Fig. 3. It is obvious that the chemical trends of the KKR results are reproduced very well by the simple model: The model calculations reproduce the parabolic behavior across the $4d$ series with the minimum at Mo where the bonding states are just filled. It should be noted, however, that the energy difference between the KKR calculations and the simple model calculations becomes very large toward the early transition-metal elements. This difference arises from the neglect of the repulsive interaction between the ionic cores, which is known to become important for the interaction between the early transition-metal atoms with a larger Wigner-Seitz radius. According to Pettifor,⁷ this repulsive interaction energy between the neighboring ion cores can be written by use of the d -electron numbers as

$$U_{\text{rep}}^{XX} = a(\dot{N}_d^X)^2 e^{-(0.87+0.15\dot{N}_d^X)R}, \quad (3.6)$$

where a ($=216$ eV) was fitted to reproduce the d -band width and Wigner-Seitz radius of the pure Mo and R is the bond length of the Ag bulk. Then the contribution of the repulsion energy $E_{\text{int}}^{\text{rep}}$ to E_{int} , due to pairing of two X impurity atoms, is given by

$$E_{\text{int}}^{\text{rep}} = U_{\text{rep}}^{XX} + U_{\text{rep}}^{AA} - 2U_{\text{rep}}^{AX}. \quad (3.7)$$

The calculated results for $E_{\text{int}}^{\text{rep}}$ and the sum total of $E_{\text{int}}^{\text{bond}}$ and $E_{\text{int}}^{\text{rep}}$ are also shown in Fig. 3. It is obvious that the differences between the KKR results and the d -bond energies are mainly attributed to the repulsive interactions. Thus we may conclude that the interaction energies of the impurity pairs of d elements in Ag mainly consists of the d - d covalent interaction between two impurities and the changes of the repulsive interactions between the ion cores.²⁴

Next, we will discuss the repulsive interaction of $5sp$ - $5sp$ impurity pairs. It can qualitatively be understood by considering the electrostatic interaction of the two impurities,^{25,26} being properly screened by the Ag host. This can be shown either by replacing the two impurity potentials by pseudopotentials and using second-order perturbation theory or by using the expression for the interaction energy derived in Ref. 4, being based on the Hellman-Feynman theorem with the nuclear charge as a variable. By treating the changes of ΔZ_1 and ΔZ_2 of the both impurities as a perturbation, the electrostatic interaction energy $E_{\text{int}}^{\text{el}}$ is in this case given by

$$E_{\text{int}}^{\text{el}} \simeq \Delta Z_1 \Delta V_2(\mathbf{R}_1) \propto \Delta Z_1 \Delta Z_2, \quad (3.8)$$

where $\Delta V_2(\mathbf{R}_1)$ is the change of the Coulomb potential at the position \mathbf{R}_1 , being induced by an isolated impurity with the excess charge ΔZ_2 at the neighboring site. The interaction is repulsive, since the potential $\Delta V_2(\mathbf{R}_1)$ for Cd-Sb impurities on the neighboring site has the same sign as ΔZ_2 ; i.e., it is repulsive for $\Delta Z_2 > 0$. This incomplete screening of the potential on the neighboring site is the reason why two sp impurities are repelling each other. It also explains directly why the In-In interaction is about

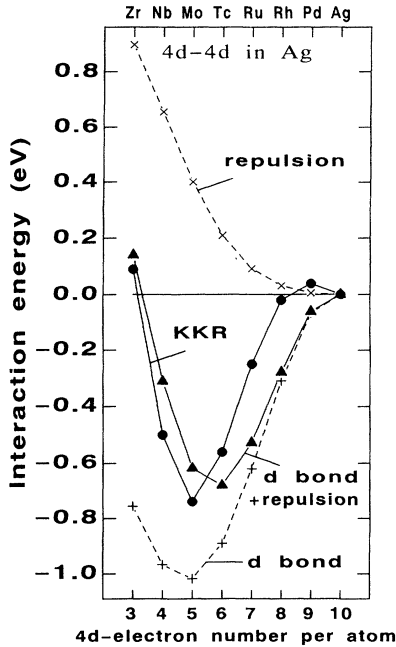


FIG. 3. Interaction energies (\blacktriangle) between two identical $4d$ impurities in Ag, obtained by the simple model calculations and two contributions: d -bond energy ($+$) and repulsion energy (\times). The results of the KKR calculations (\bullet) are also shown for comparison.

4 times larger than the Cd-Cd interaction. Of course, the above expression for the interaction is based on perturbation theory and only holds for small ΔZ_i 's. For higher valent impurities, Eq. (3.8) is no longer valid. The covalent interaction between the $5sp$ orbitals at two impurities, which is not included in the approximate formula (3.8), also becomes important; it is attractive and cancels a main part of the repulsion due to the electrostatic interaction. Consequently, one may expect the smooth change of the interaction energies from In to Sb. A more detailed discussion of the trends of the interaction energies will be given elsewhere.²⁴ Note that in the above discussion the d band of Ag does not enter at all. We believe that it plays a minor role in the interaction, so that for this purpose the Ag host might be well described by a jellium model.

B. Impurity-impurity interactions in a transition-metal Pd

The calculated nearest- and next-nearest-neighbor interaction energies of the $4d$ and $5sp$ impurity pairs in Pd are shown in Fig. 4 and Table I. We also note that the next-nearest-neighbor interaction energies are very small compared to the nearest-neighbor interactions. It is found from a detailed comparison between Tables I and II that the differences between the segregation and solid solution behavior of the corresponding binary alloys,^{1,17-19} known experimentally, can be explained by considering only the dominating nearest-neighbor interaction: An attractive interaction leads to segregation, a repulsive one to a solid solution. In all cases the theory explains the observed experimental behavior (see Secs. III and V).

It should be noted from the comparison between Figs. 2 and 4 that the fundamental trends of the interactions in Pd are rather similar to those in Ag, although the in-

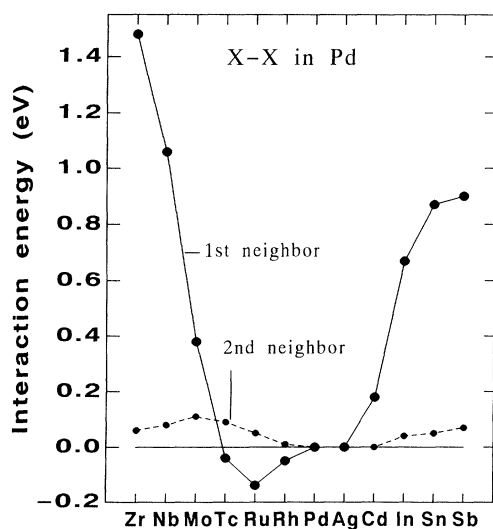


FIG. 4. Interaction energies between two identical $4d$ or $5sp$ impurities in Pd. The large solid circles (●) indicate the interaction energies for the nearest-neighbor sites, and the small solid circles (●) refer to the next-nearest-neighbor sites.

teractions are much more repulsive in Pd than in Ag: The strong attraction in the middle of the $4d$ series disappears for the Pd host, and the repulsive interactions for the early $4d$ impurities and also for $5sp$ impurities are much stronger in Pd. The disappearance of the strong attraction in the $4d$ impurity region can be explained by considering, in addition to the $d-d$ bond between the two impurities, the energy loss due to the breakup of two d bonds between the host orbitals and the $4d$ impurity orbitals, which occurs as a result of the impurity pair formation. This effect can be neglected in the Ag host because the bonding between the impurities and host atoms is rather weak, as discussed in Sec. III A. According to the Alexander-Anderson model discussed in the previous subsection, the energy loss due to the breakup of two d bonds between the Pd and impurity atoms becomes very large for the early transition-metal impurities.²⁴ It is the largest for the Pd-Y pair as the system is characterized by strongly covalent bonding. Since the total $4d$ electron number of the Pd-Y pair is ~ 10 , the low-lying bonding states are fully occupied, leading to an optimal bond strength and consequently a very large bond-breaking energy. The strong repulsion of $5sp-5sp$ pairs in Pd can be explained along similar lines: By forming the pair, two rather strong $5sp-4d$ bonds between the $5sp$ impurities and the Pd host must be broken. This energy loss is not overcome by the energy gain due to the formation of the weak $5sp-5sp$ bond between both impurities and the additional Pd-Pd bond; the special strength of the $5sp-4d$ bonds of $5sp$ impurities in Pd can be estimated from the large solution energies in Pd (see Fig. 4 in Ref. 5). For these reasons the interaction energies of $5sp$ impurities in Pd are repulsive.

IV. CALCULATED RESULTS OF THE IMPURITY PAIRS IN Cu AND Ni

In this section we discuss the calculated results for the nearest- and next-nearest-neighbor interaction energies of the impurity pairs Sc to As in Cu and Ni. The electronic structures for the ground states of impurity pairs of Sc to V, Ni, and Zn to As in Cu are nonmagnetic, but magnetic for the impurity pairs of Cr to Co in Cu and all the impurity pairs in Ni. The microscopic mechanisms of the impurity-impurity interactions can be explained similarly as discussed in the previous section, except for the strongly magnetic impurity pairs of Cr to Co, where the changes of the local moments due to pairing of the impurities becomes important.

A. Impurity-impurity interactions in a noble metal Cu

Figure 5 and Table III show the calculated interaction energies of these impurity pairs (Sc to As) in Cu. Table III also includes the results for Ni, being discussed later. For the comparison with the results of the $4d$ impurity pairs in Ag, being nonmagnetic, the calculated results without spin polarization are also shown in Fig. 5. Again, it is obvious that the nearest-neighbor interaction is dominating. We find from a detailed comparison be-

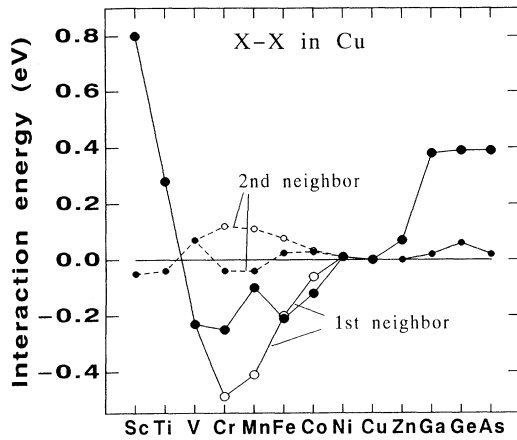


FIG. 5. Interaction energies between two identical 3d or 4sp impurities in Cu. The large solid circles (●) indicate the interaction energies for the nearest-neighbor sites, and the small solid circles (●) refer to the next-nearest-neighbor sites. Open circles (○ and ○) refer to calculations without spin polarization.

tween Tables II and III that the observed fundamental characteristic features of the phase diagrams^{1,17-19} can qualitatively be explained by the nearest-neighbor interaction of the impurity pairs: The attractive interaction leads to segregation, the repulsive one to a solid solution (see Sec. III). By comparison of the results of Fig. 2 for Ag and Fig. 5 for Cu, we see that the characteristic features are very similar, except for the impurities Cr, Mn, Fe, and Co, which are magnetic.

Here we will therefore only discuss the magnetism of the nearest-neighbor impurity pairs of Cr to Co in Cu. The ground states of the impurity pairs are antiferromagnetic for Cr and Mn and ferromagnetic for Fe and Co. The existence of an antiferromagnetic configuration for Mn and of a ferromagnetic configuration for Fe is in agreement with neutron-scattering measurements of Davis, Burke, and Rainford.²⁷ The magnetic moments for the impurity pairs as well as the isolated impurities

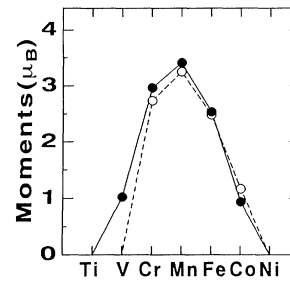


FIG. 6. Local moments of the isolated 3d impurities (●) and the 3d impurity pairs (○) in Cu. The Cr and Mn impurity pairs have antiferromagnetic configurations, and the Fe and Co impurity pairs have the ferromagnetic configurations.

are shown in Fig. 6: a vanishing moment for the V pair, a considerable decrease (-0.22 and -0.16) for the antiferromagnetic configurations of Cr and Mn, a small decrease (~ -0.05) for the ferromagnetic configuration of Fe, and a considerable increase (0.24) for the ferromagnetic configuration of Co. The behavior of the moment changes due to pairing can easily be understood by use of the Alexander-Anderson model combined with second-order perturbation of the covalent interaction matrix elements.⁶ For the antiferromagnetic case the moments always decrease, while for the ferromagnetic case the moments decrease or increase depending on the derivative of the local densities of the states at the Fermi level. For example, the small change of the moments of Fe is easily explained by considering the peak position of the density of states of the minority spin: Since the peak is located at the Fermi level, the splitting of the minority peak cannot change the moment.⁶ These moment changes lead to a complicated behavior of interactions for the strong magnetic impurity pairs. If we use the tight-binding approximation and assume charge neutrality, the changes of the binding energy (per two impurity atoms) due to the changes of the magnetic moments may be written as

TABLE III. Calculated n th-neighbour interaction energies E_n^{int} ($n=1,2$) of 3d and 4sp impurity pairs (Sc to As) in Cu (in eV). The ground states for the nearest-neighbor (next-nearest-neighbor) impurity pairs in Cu are antiferromagnetic (ferromagnetic) for Cr and Mn and ferromagnetic (antiferromagnetic) for Fe and Co. For the other nearest- and next-nearest-neighbor impurity pairs in Cu, the ground states are nonmagnetic. The ground states of the impurity pairs in Ni are ferromagnetic for all the impurity pairs of the nearest-neighbor as well as the next-nearest neighbor. For Cr to Co impurities in Cu, the interaction energies of the excited states are also shown in parentheses; the excited states for the nearest-neighbor (next-nearest-neighbor) impurity pairs are ferromagnetic (antiferromagnetic) for Cr and Mn and antiferromagnetic (ferromagnetic) for Fe and Co. Negative values mean attractive, positive ones repulsive interaction.

Impurity	Sc	Ti	V	Cr	Mn	Fe	Co	Ni	Cu	Zn	Ga	Ge	As
	Host Cu												
E_1^{int}	0.80	0.28	-0.23	-0.25	-0.10	-0.21	-0.12	0.01		0.07	0.38	0.39	0.39
				(0.12)	(0.07)	(-0.05)	(-0.04)						
E_2^{int}	-0.05	-0.04	0.07	-0.04	-0.04	0.03	0.03	0.01		0.00	0.02	0.06	0.02
				(0.03)	(0.03)	(0.04)	(0.04)						
Host Ni													
E_1^{int}	0.90	0.81	0.45	0.01	0.22	0.13	0.00		-0.02	0.09	0.35	0.66	0.69
E_2^{int}	-0.02	-0.10	-0.15	-0.15	0.01	-0.01	0.00		0.00	0.01	0.01	0.02	0.02

$$\Delta E_{\text{mag}} = -\frac{J}{2} \{ (M + \Delta M)^2 - M^2 \}, \quad (4.1)$$

where J and M are the exchange integral and magnetic moment for the single impurity; ΔM is a change of the magnetic moment due to pairing of two impurities. If we use the KKR results for the magnetic moments, the magnetic part of the interaction acts repulsively for the Cr and Mn pairs and attractively for the Co pairs. For the Fe pairs, it will be weak since the magnetic moment is practically unchanged, as seen in Fig. 5. If J is assumed to be ~ 0.6 eV,²⁸ ΔE_{mag} is 0.39, 0.33, 0.08, and -0.15 eV for Cr, Mn, Fe, and Co, corresponding to the KKR results of 0.24, 0.31, -0.01 , and -0.06 eV. The differences of the simple model calculations with the KKR results may be attributed to the changes of the kinetic energies due to the changes of the wave functions, being also caused by pairing of two impurities.

B. Impurity-impurity interactions in a transition metal Ni

Figure 7 and Table III show the calculated interaction energies of the impurity pairs Sc to As in Ni. It is also true that the observed fundamental characteristic features of the phase diagrams, as listed in Table II, can be almost explained by the nearest-neighbor interaction of the impurity pairs: The attractive interaction leads to segregation, the repulsive one to a solid solution (see Secs. III and V). We note from the comparison between Figs. 4 and 7 that the characteristic features of the nearest-neighbor interaction energies of the $3d$ and $4sp$ impurity pairs in Ni are similar to those of the $4d$ and $5sp$ impurity pairs in Pd, although there are considerable differences in details: (1) the weak repulsion for Mn and Fe in Ni compared with the weak attraction for Tc, Ru, and Rh in Pd and (2) the considerable reduction of the repulsive interactions for the early $3d$ and $4sp$ impurities in Ni, com-

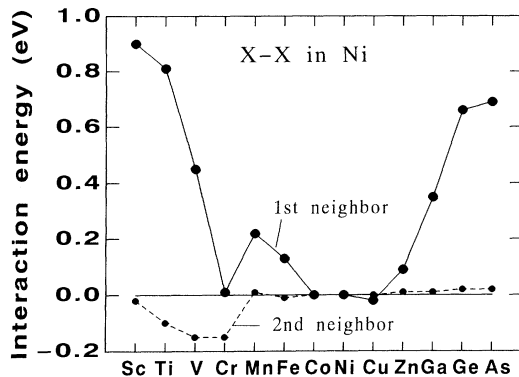


FIG. 7. Interaction energies between two identical impurities of the $3d$ or $4sp$ impurities in Ni. The large solid circles (●) indicate the interaction energies for the nearest-neighbor sites, and the small solid circles (●) refer to the next-nearest-neighbor sites. All the impurity pairs have ferromagnetic configurations; the impurity moment couples ferromagnetically to the host moment from Mn to Co and otherwise antiferromagnetically to the host moment.

pared with the early $4d$ and $5sp$ impurities in Pd. The first difference can be explained by considering the decrease of the impurity moments due to pairing: The moments for Mn, Fe, and Co change from 2.90, 2.68, and 1.71 to 2.80, 2.62, and 1.69; the impurity pairs prefer the ferromagnetic configurations and couple ferromagnetically to the host moment. We also note that the changes of the moments of the host Ni atoms adjacent to the impurities are very small.²⁹ As a result, we may expect that the changes of the impurity moments due to pairing act repulsively for Mn, Fe, and Co, as discussed for Cr and Mn in Cu. In contrast to this, the reduction of the repulsive interaction of the early $3d$ impurities in Ni is presumably due to the weaker hybridisation of the $3d$ orbitals compared with the $4d$ ones,²² which decreases the bond strength between the host atom and the impurity. Magnetic effects presumably do not play a role here.

V. INTERACTION ENERGIES AND PHASE DIAGRAM

The present approach to the impurity-impurity interactions in Cu, Ni, Ag, and Pd has yielded *ab initio* predictions which can be used for calculating alloy properties such as ordering and segregation and, in principle, also phase diagrams. In order to determine equilibrium configurations at finite temperatures, we relate the impurity pair energies E_1 and E_2 to the effective pair interactions $E = -4J$ of the Ising model

$$H = - \sum_{i,j} ' J_{ij} s_i s_j ,$$

with the occupation variable $s_i = \pm 1$ if either atom A or B is at site i and \sum' avoids double counting.³⁰ Since the impurity pair energies have been obtained for the dilute limit and the variation of these energies with composition is *a priori* not known, and since, moreover, only the interactions of the first and second neighbors are calculated, the predictive power of the present results concerning alloy properties might be limited and it is interesting to see how well one is doing.

The following discussions will compare the present calculations with experimental data. First, Table II summarizes the ordering and decomposition properties as obtained from the phase diagrams of the host-impurity alloys being considered here. Second, Fig. 8 shows which ordered alloy phases may be expected to form on the fcc lattice (even if the fcc phase does not remain stable with alloying, one might predict the metastable fcc phases, for instance, Gruinier-Preston zones). Third, the solid solubilities of the impurities are related to the impurity interactions (see Table II). If, for instance, E_1 or E_2 is negative, the solubility is typically small and analytically determined, while, if both E_1 and E_2 are positive, the solubility should be larger even at lower temperatures (as calculated by Monte Carlo simulations). Finally, we discuss the impurity interactions in view of the results for concentrated alloys investigated by diffuse-scattering measurements and KKR-CPA-GPM (a combination of generalized perturbation method with the Korringa-Kohn-Rostoker multiple-scattering formulation of the

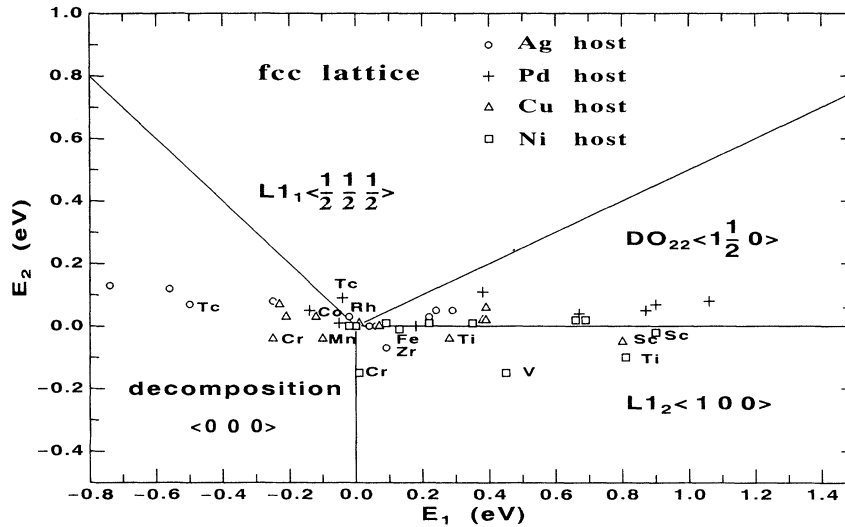


FIG. 8. Distribution of the ordered structures as a function of E_1 and E_2 . One clustering family and three types of ordering families appear if the interactions are taken into account up to the second neighbor: (1) $\langle 000 \rangle$, decomposition; (2) $\langle 100 \rangle$, Cu_3Au structure (L_2); (3) $\langle 1\frac{1}{2}0 \rangle$, Al_3Ti structure (DO_{22}); and (4) $\langle \frac{1}{2}\frac{1}{2}\frac{1}{2} \rangle$, CuPt structure (L_1). The calculated impurity-impurity interactions in Cu, Ni, Ag, and Pd are shown for comparison with the experimentally observed structures.

coherent-potential approximation) calculations.

Since the nearest-neighbor interaction is rather dominating, its sign already determines whether ordered compounds should be formed or a miscibility gap should be observed experimentally, discussed in Secs. III and IV. The results obtained are in remarkable agreement with the experimental phase diagrams (see Table II). Furthermore, large values of E_1 are confirmed by the ordered structures, which are stable up to the melting point. Since there is a rather good general agreement, we discuss only the very few discrepancies. In the case of AgZr , the calculated interactions are not sufficiently strong to explain the stability of the ordered phases, indicating that probably further long-range interactions exist. At first sight the observed ordering tendency of Mn impurities in Cu seems to contradict the calculations. However, if the energies of the ferromagnetic and antiferromagnetic Mn configurations are considered (see Table III) and the magnetic contribution to the chemical ordering is fully taken into account (see discussion of CuCo further below), ordering is indeed to be expected. No phase diagram is available for AgTc , where we would predict a miscibility gap.

Second, we discuss the particular possible ordered structures which could be formed in the more concentrated fcc-based alloys. Therefore even the typically small second-neighbor interactions are of importance. Of course, the interactions to further neighbors, being not calculated in the present work, may be important as well.³¹ Considering the phase stabilities of ordered structures based on first- and second-neighbor interactions, four types ordering families for the fcc alloys can be distinguished. The absolute minima of the interaction potential $E(\mathbf{h})$ are located at the four high-symmetry points in the reciprocal space of the fcc lattice. Therefore one expects, in the case of an ordering wave vector \mathbf{h} ,³² (1) $\mathbf{h} = \langle 000 \rangle$, simple phase decomposition; (2) $\mathbf{h} = \langle 100 \rangle$, Cu_3Au structure (L_2); (3) $\mathbf{h} = \langle 1\frac{1}{2}0 \rangle$, Al_3Ti structure (DO_{22}); and (4) $\mathbf{h} = \langle \frac{1}{2}\frac{1}{2}\frac{1}{2} \rangle$, CuPt structure (L_1).

The distribution of the ordered structures as a function of E_1 and E_2 is represented in Fig. 8. The alloys of the $\langle 000 \rangle$ region do indeed show phase decomposition, as expected. Peculiarly, almost all results for these alloys have a positive (repulsive) E_2 . We briefly note that this will influence the manner of phase separation: From Monte Carlo simulations, we found that the (100) interfaces tend to flatten during the process of decomposition.

The distinction into the three different ordering families turns out to be less successful. Predominantly, this is caused by ordering on other basic lattices than the assumed fcc structure. Therefore a prediction of such incoherent phase transformations is not possible on the basis of the present data alone. As an example, alloys which are expected to belong to the ordering family $\langle 100 \rangle$ show often a different behavior; Sc and Ti impurities in Cu and Ni reveal a very strong ordering tendency, but form ordered structures on a hcp rather than on the fcc lattice.^{1,19} Two further candidates for a Cu_3Au structure are Cr and V impurities in Ni. However, these alloys make the DO_{22} structure.^{30,33} As discussed later, experimental data on the interaction energies indicate the importance of further-neighbor interactions (see Table IV). Only the alloys Ni_3Fe really form the Cu_3Au structure as suggested in Fig. 8.^{1,19} Alloys with E_1 and E_2 positive are expected to order in the DO_{22} structure. However, in particular, for large values of E_1 and E_2 the alloys form an ordered structure but not anymore on the basic fcc lattice. This can be understood in view of the frustration effects due to positive E_1 and E_2 . Changing the the basic lattice structure—typically to hcp—may then lead to energetically more favored ordered structures. The DO_{22} structure seems to be only likely for small interaction energies. Concerning $\langle \frac{1}{2}\frac{1}{2}\frac{1}{2} \rangle$ ordering family, our results indicate only the two possible candidates AgRh and PdTc . However, no certain experimental information about PdTc is available, and AgRh appears to be insoluble (although this could stem from the

TABLE IV. Interaction energies determined from diffuse-scattering experiments by use of the inverse Monte Carlo method (in eV). For Ni₃Fe, only the ferromagnetic configurations are taken into account to analyze the experimental results (see text).

	Ni ₃ V ^a	Pd ₃ V ^a	Ni ₃ Fe ^b	Ni _{0.89} Cr _{0.11} ^c	Ni _{0.59} Cu _{0.41} ^b	CuZn ^d	
						$c_{Zn}=0.311$	$c_{Zn}=0.224$
E_1	0.124	0.180	0.052	0.052	-0.024	0.037	0.047
E_2	-0.058	-0.006	-0.022	-0.021	0.011	-0.013	-0.003
E_3	-0.022	0.023	0.000	-0.003	0.000	-0.003	
E_4	0.012	0.026	0.000	0.026	0.000	0.000	

^aReference 33.

^bReference 40.

^cReference 30.

^dReference 37.

insolubility in the molten alloys).^{1,19}

Third, we discuss measured solid solubilities of impurities which may serve as a stringent test of the calculated interaction energies. Remaining differences should indicate the necessity of extending the present interaction model; for instance, it may imply that further than second-neighbor interactions are required for quantitative agreement and also that the contributions to the energies due to the lattice distortions, being neglected in the present calculations, are important. It is worthwhile to note that there are qualitative differences in the solubilities related to the above-mentioned different cases of ordering. Assuming an approximation for the dilute limit, the boundary of solubility x is determined by $x = \exp[(6E_1 + 3E_2)/k_B T]$ for the simple phase decomposition $\langle 000 \rangle$, while for the Cu₃Au structure $\langle 100 \rangle$ the boundary is given by $x = \exp(3E_2/k_B T)$.

Such analytic approximations fail to describe the solubility boundary for alloys belonging to the $\langle 1\frac{1}{2}0 \rangle$ region; regarding the distribution of results in Fig. 8, this concerns a major part of the results. Even at $T=0$ there is a large solubility, due to the merely repulsive character of the impurity interactions. From Monte Carlo simulations by one of us, the solubility at $T=0$ has been calculated to $x=0.0836$ for this case, where both E_1 and E_2 are positive. If $E_2=0$, this describes the boundary between $\langle 100 \rangle$ and $\langle 1\frac{1}{2}0 \rangle$; the Monte Carlo result of the solubility boundary at $T=0$ is even larger: $x=0.111$. Therefore the signs of the interaction energies E_1 and E_2 distinguish not only the possible ordered ground states (see Fig. 8), but furthermore also the characteristics of the impurity solubilities. The comparison between the measured solubilities and such quantitative predictions is given in Table II (although the numerical values are not listed) and yields a favorable agreement.

Quantitative comparisons seem to be successful only for the solubilities of the segregating alloys, where the dominating interaction $E_1 (<0)$ is also playing a role. Calculated and experimental values agree well in the same order of magnitude. This seems to be a modest agreement, at least at first sight. However, since x depends exponentially upon the E 's, this is a quite satisfactory result. Deviations expressed in terms of the interaction energies, presumably to further neighbors, are typi-

cally not larger than 0.02 eV. One exceptionally good result for Co impurities in Cu will now be described in further detail, since it also illustrates the influence of magnetism. We note first that they are not the energies of the nonmagnetic configurations—highest excited state—which determine the effective chemical interactions and therefore the solubility boundary. Rather, from the interaction energies E_F and E_A corresponding to the ferromagnetic (ground state) and antiferromagnetic (lowest excited state) configurations of a Co-Co pair, respectively, one obtains the chemical interaction $E_{ch} [= (E_A + E_F)/2]$ and the magnetic exchange interaction $E_{mag} (= E_A - E_F)$: $E_{ch,1} = -0.0802$ eV, $E_{ch,2} = 0.0329$ eV, $E_{mag,1} = 0.0777$ eV, and $E_{mag,2} = -0.01025$ eV. Then, using these parameters, a Monte Carlo simulation has yielded an almost perfect agreement with accurate measured solubilities;³⁴ one can estimate the possible contribution from E_3 to be as small as 0.003 eV.

The situation turns out to be rather complicated if both the host and impurity elements are magnetic, for instance, in the case of Fe or Cr impurities in Ni; although, in principle, a Monte Carlo calculation for the finite-temperature properties is feasible, it requires the following condition and calculations: (1) The moments must be stable against rotations, and (2) the exchange energies between all pairings of moments belonging to the host and impurity elements must be calculated.

Last, we discuss the impurity interactions obtained from diffuse-scattering measurements and KKR-CPA-GPM calculations. We have only a few examples of alloys, where the interaction energies have been determined from diffuse-scattering data which can be used for direct comparisons (see Table IV). There are large discrepancies between the calculated interactions of V impurities in Ni ($E_1=0.45$ eV and $E_2=-0.15$ eV for $c_V=0.25$; see Table III) and the values deduced from scattering experiments on disordered Ni₃V [$E_1=0.124$ eV and $E_2=-0.058$ eV for $c_V=0.25$ (Ref. 33)] as well as between those of V impurities in Pd [$E_1=0.48$ eV and $E_2=0.07$ eV for $c_V=0$ (Ref. 35)] and the values deduced from scattering experiments on disordered Pd₃V ($E_1=0.180$ eV and $E_2=-0.006$ eV for $c_V=0.25$), which cannot be explained by error bars of any of the methods;

it should be noted that the calculated results are the interaction energies for the dilute limit, while the experimental results correspond to the concentrated alloys of $c_V=0.25$. Therefore a strong concentration dependence for the interactions might be inferred. This may be seen in the KKR-CPA-GPM results for the PdV alloy;³⁶ while the results in the 25% V region agree well with the experimental ones, for smaller concentrations the interaction energies increase and are boldly extrapolated to the dilute limit values of $E_1 \sim 0.4$ eV and $E_2 \sim 0.1$ eV, which are in good agreement with the present calculations (0.48 and 0.07 eV).

By similar comparison for the interaction energies for the CuZn alloy, one obtains a fairly good agreement between the diffuse-scattering experiments [$E_1=0.047$ eV and $E_2=-0.003$ eV for $c_{Zn}=0.224$, $E_1=0.037$ eV and $E_2=-0.013$ eV for $c_{Zn}=0.311$ (Ref. 37)], the KKR-CPA-GPM calculations [$E_1=0.06$ eV and $E_2=-0.014$ eV for $c_{Zn}=0-0.5$ (Refs. 38 and 39)], and ours calculations ($E_1=0.07$ eV and $E_2=0.00$ eV for $c_{Zn}=0$; see Table III), within deviations of 0.03 eV. According to the KKR-CPA-GPM calculations, there is no significant concentration dependence up to $c_{Zn}=0.5$. This trend is clearly supported by the agreement of our calculations for a dilute limit with the experimental results for the concentrated alloys ($c_{Zn}=0.224$ and 0.311).

For NiCu, the diffuse-scattering data⁴⁰ yield very small interaction energies ($E_1=-0.024$ eV and $E_2=0.011$ eV for $c_{Zn}=0.41$), as also expected from the phase diagrams showing a continuous solubility and consistent with the present calculations for the dilute limit ($E_1=-0.02$ eV and $E_2=0.00$ eV for Cu impurities and $E_1=0.01$ eV and $E_2=0.01$ eV for Ni impurities). For NiCr, the differences between our results ($E_1=0.01$ eV and $E_2=-0.15$ eV for $c_{Cr}=0$; see Table III) and those of the diffuse-scattering experiments³⁰ ($E_1=0.052$ eV and $E_2=-0.021$ eV for $c_{Cr}=0.11$) are larger. However, it is not surprising because the magnetic properties of Ni are strongly reduced with the increasing Cr content; therefore, the ground-state energies of Cr impurity pairs in Ni cannot be expected to describe the effective interactions in the concentration alloys.³⁰

VI. SUMMARY AND CONCLUSION

The aim of this paper was to present accurate data for the nearest- and next-nearest-neighbor interactions of impurity pairs in Cu, Ni, Ag, and Pd and to elucidate the physical mechanisms responsible for the interaction. In order to minimize the effect of lattice relaxations, not included in the present calculations, we considered only combinations of hosts and impurities from the same row of the periodic table. We applied density-functional theory in the local-density approximation and solved the Kohn-Sham equations by using the KKR Green's-function method for impurity calculations.²⁻⁵

The strong attraction of 4*d* impurities in Ag is due to the covalent interaction between the 4*d* orbitals, while the repulsion of 5*sp*-5*sp* pairs can be explained by the electrostatic interaction between the excess charges of the impurities; this is a similar mechanism as discussed for the vacancy-solute interactions in Ag.⁴ For Pd, the attractive interaction is very weak in the middle of the 4*d* series because the energy loss due to the breakup of the *d* bonds between the host and impurity atoms cannot be overcome by the energy gain due to the formation of *d-d* bonds between the two 4*d* impurities. The stronger repulsion for 5*sp*-5*sp* pairs in Pd than in Ag can be explained by the formation of strong 4*d*-5*sp* bonds being broken up by aggregation. The fundamental microscopic mechanisms of the interactions of the 3*d* and 4*sp* impurity pairs in Cu and Ni are almost the same as those of the interactions of the 4*d* and 5*sp* impurity pairs in Ag and Pd, except for the cases of strongly magnetic impurities. It has been shown that, for the impurity pairs (Cr to Co) in Cu as well as for the late 3*d* impurity pairs in Ni, the magnetic contribution to the impurity-impurity interactions can be explained by the changes of the impurity moments on pairing. In contrast to these, for the early 3*d* impurity pairs in Ni, the weaker hybridization of the 3*d* orbitals reduces the repulsive interaction.

In practically all cases considered, we find that the first-nearest neighbor interaction dominates the alloy behavior: An attractive nearest-neighbor interaction of the pair leads to segregation, a repulsive interaction to ordering. This simple rule is in good agreement with phase-diagram information. However, otherwise a comparison with experiments is very difficult. For ordering alloys the ordered structures as predicted by our calculations are often not found because other structures, e.g., those based on the hcp instead of fcc, are more stable. Estimations for solid solubilities of impurities are somewhat more successful, especially for CuCo. For CuZn we obtain good agreement with diffuse-scattering measurements and KKR-CPA-GPM calculations, while for NiV and PdV the comparison points to an unusual large concentration dependence of the interaction.

ACKNOWLEDGMENTS

We want to thank B. Drittler and A. Carlsson for very useful discussions. One of the authors (T.H.) would like to thank T. Asada and K. Terakura for many helpful discussions. The main part of the present results on the basis of the KKR-Green's-function method has been obtained by use of a Cray-XMP computer at Forschungszentrum Jülich, and the model calculations to analyze the KKR results were carried out with the computers at Institute for Molecular Science (Okazaki, Japan). This work is partly supported by a Grand-in-Aid for Scientific Research from Japanese Ministry of Education, Science and Culture.

- ¹F. R. de Boer, R. Boom, W. C. Mattens, A. Miedema, and A. K. Niessen, in *Cohesion in Metals*, edited by F. R. de Boer and D. G. Pettifor (North-Holland, Amsterdam, 1985), Vol. 1.
- ²P. J. Braspenning, R. Zeller, A. Lodder, and P. H. Dederichs, *Phys. Rev. B* **29**, 703 (1984).
- ³B. Drittler, M. Weinert, R. Zeller, and P. H. Dederichs, *Phys. Rev. B* **39**, 930 (1989).
- ⁴U. Klemradt, B. Drittler, R. Zeller, and P. H. Dederichs, *Phys. Rev. Lett.* **64**, 2803 (1990); U. Klemradt, B. Drittler, T. Hoshino, R. Zeller, P. H. Dederichs, and N. Stefanou, *Phys. Rev. B* **43**, 9487 (1991).
- ⁵T. Hoshino, B. Drittler, R. Zeller, and P. H. Dederichs, *Phys. Rev. B* **45**, 12 202 (1992).
- ⁶A. Oswald, R. Zeller, P. J. Braspenning, and P. H. Dederichs, *J. Phys. F* **15**, 193 (1985).
- ⁷D. G. Pettifor, in *Solid State Physics*, edited by H. Ehrenreich and D. Turnbull (Academic, New York, 1987), Vol. 40, p. 43.
- ⁸For a review, see A. Gonis, M. Sluiter, P. E. A. Turchi, G. M. Stocks, and D. M. Nicholson, *J. Less-Common Met.* **168**, 127 (1991).
- ⁹J. W. Connolly and A. R. Williams, *Phys. Rev. B* **27**, 5169 (1983); Z. W. Lu, S.-H. Wei, A. Zunger, S. Frota-pessoa, and L. G. Ferreira, *ibid.* **44**, 512 (1991).
- ¹⁰F. Ducastelle and F. Gautier, *J. Phys. F* **6**, 2039 (1976).
- ¹¹N. Stefanou, R. Zeller, and P. H. Dederichs, *Solid State Commun.* **62**, 735 (1987).
- ¹²R. Kikuchi, *Phys. Rev.* **81**, 988 (1951); J. M. Sanchez, F. Ducastelle, and D. Gratias, *Physica A* **128**, 334 (1984).
- ¹³K. Binder, J. L. Lebowitz, M. H. Phani, and M. H. Kalos, *Acta Metall.* **29**, 1655 (1981).
- ¹⁴R. Zeller, J. Deutz, and P. H. Dederichs, *Solid State Commun.* **44**, 993 (1982).
- ¹⁵U. Klemradt, diploma thesis, Technical University Aachen, Aachen, Germany, 1989.
- ¹⁶V. L. Moruzzi, J. F. Janak, and A. R. Williams, *Calculated Electronic Properties of Metals* (Pergamon, New York, 1978).
- ¹⁷R. Hultgren, P. D. Desai, D. T. Hawkins, M. Gleiser, and K. Kelly, *Selected Values of Thermodynamic Properties of Metals and Alloys* (American Society of Metals, Metal Park, OH, 1973).
- ¹⁸O. Kubaschewsky and C. B. Alcock, *Metallurgical Thermochemistry* (Pergamon, Oxford, 1979).
- ¹⁹*Constitution of Binary Alloys*, edited by M. Hansen and K. Anderko (McGraw-Hill, New York, 1958); *Constitution of Binary Alloys: First Supplement*, edited by R. P. Elliot (McGraw-Hill, New York, 1965); *Constitution of Binary Alloys: Second Supplement*, edited by F. A. Shunk (McGraw-Hill, New York, 1969); W. G. Moffat, *Handbook of Binary Phase Diagrams* (Genium, Schenectady, NY, 1980); T. B. Massalski, *Binary Alloy Phase Diagrams*, 2nd ed. (ASM International, New York, 1990).
- ²⁰S. Alexander and P. W. Anderson, *Phys. Rev.* **133**, A1594 (1964).
- ²¹V. Heine, *Phys. Rev.* **153**, 673 (1967).
- ²²W. A. Harrison and S. Froyen, *Phys. Rev. B* **21**, 3214 (1980).
- ²³W. A. Harrison, *Electronic Structure and the Properties of Solids* (Freeman, San Francisco, 1980).
- ²⁴T. Hoshino, R. Zeller, and P. H. Dederichs (unpublished).
- ²⁵A. Blandin, J. L. Deplante, and J. Friedel, *J. Phys. Soc. Jpn.* **18**, Suppl. II, 85 (1963).
- ²⁶J. L. Deplante and A. Blandin, *J. Phys. Chem. Solids* **26**, 381 (1965).
- ²⁷J. R. Davis, S. K. Burke, and B. D. Rainford, *J. Magn. Magn. Mater.* **15-18**, 151 (1980).
- ²⁸R. Podloucky, R. Zeller, and P. H. Dederichs, *Phys. Rev. B* **22**, 5777 (1980).
- ²⁹N. Stefanou, A. Oswald, R. Zeller, and P. H. Dederichs, *Phys. Rev. B* **35**, 6911 (1987).
- ³⁰W. Schweika and H. G. Haubold, *Phys. Rev. B* **37**, 9240 (1988).
- ³¹J. Kanamori and Y. Kakehashi, *J. Phys. (Paris) Colloq.* **38**, C7-274 (1977).
- ³²P. C. Clapp and S. C. Moss, *Phys. Rev.* **171**, 754 (1968).
- ³³R. Caudron, M. Sarfati, M. Barrachin, A. Finel, F. Ducastelle and F. Solal, *J. Phys. (Paris)* (to be published).
- ³⁴G. Tammann and W. Oelsen, *Z. Anorg. Allg. Chem.* **186**, 257 (1930).
- ³⁵We also calculated the impurity-impurity interactions of a V-V pair in Pd, yielding $E_1 = 0.48$ eV, $E_2 = 0.07$ eV.
- ³⁶P. E. A. Turchi, G. M. Stocks, W. H. Butler, D. M. Nicholson, and A. Gonis, *Phys. Rev. B* **37**, 5982 (1988).
- ³⁷L. Reihard, B. Schönfeld, G. Kistorz, and W. Bührer, *Phys. Rev. B* **41**, 1727 (1990).
- ³⁸M. Sluiter, P. E. A. Turchi, D. D. Johnson, F. J. Pinski, D. M. Nicholson, and G. M. Stocks, in *Neutron Scattering for Materials Science*, edited by S. M. Shapiro, S. C. Moss, and J. D. Jorgensen, MRS Symposia Proceedings No. 166 (Materials Research Society, Pittsburgh, 1990), p. 225.
- ³⁹P. E. A. Turchi, M. Sluiter, F. J. Pinski, D. D. Johnson, D. M. Nicholson, G. M. Stocks, and J. B. Staunton, *Phys. Rev. Lett.* **67**, 1779 (1991).
- ⁴⁰W. Schweika, in *Alloy Phase Stability*, edited by G. M. Stocks and A. Gonis (Kluwer Academic, Dordrecht, 1989), p. 147.